remote sensing

Technical Note

Preliminary Evaluation of FY-3E Microwave Temperature Sounder Performance Based on Observation Minus Simulation

Xiaoli Qian [1], Zhengkun Qin [1], Juan Li [2,3,*], Yang Han [2,3] and Guiqing Liu [2,3]

1 Joint Center for Data Assimilation for Research and Application, Nanjing University of Information Science and Technology, Nanjing 210044, China; 20191201014@nuist.edu.cn (X.Q.); qzk_0@nuist.edu.cn (Z.Q.)
2 CMA Earth System Modeling and Prediction Centre, Beijing 100081, China; hanyang@cma.gov.cn (Y.H.); liugq@cma.gov.cn (G.L.)
3 State Key Laboratory of Severe Weather, Chinese Academy of Meteorological Sciences, Beijing 100081, China
* Correspondence: lj@cma.gov.cn

Abstract: The FY-3E satellite was successfully launched on 5 July 2021 and carries on board the Microwave Temperature Sounder-III (MWTS-III). In this study, the biases of MWTS-III data with respect to simulations are analyzed according to the instrument field of view and location latitude over the Pacific region. The cloud liquid water path (CLWP) over oceans is retrieved from two new window channels at 23.8 and 31.4 GHz and is used for detecting the clouds-affected microwave sounding data. The absolute bias between the observed and simulated brightness temperature (O–B) under the clear sky point is, in general, less than 2.0 K, depending on the MWTS-III channel. The standard deviations of O-B in most channels are less 1.0 K, but they are 1–1.5 K in channels 1–4 and 17. The average and the standard deviation of O−B from the channels 1–10 shows an obvious symmetrical variation with FOV. The evaluation results all indicate good prospects for the assimilation application of FY-3E microwave sounding data.

Keywords: FY-3E; MWTS; radiative transfer for TOVS; field of view; CLWP

check for updates

Citation: Qian, X.; Qin, Z.; Li, J.; Han, Y.; Liu, G. Preliminary Evaluation of FY-3E Microwave Temperature Sounder Performance Based on Observation Minus Simulation. *Remote Sens.* **2022**, *14*, 2250. https://doi.org/10.3390/rs14092250

Academic Editor: Simone Lolli

Received: 29 March 2022
Accepted: 5 May 2022
Published: 7 May 2022

1. Introduction

Satellite observations have become one of the main sources of meteorological observation data and are widely used in numerical weather prediction models. Among all the satellite data, the assimilation of the polar-orbiting satellite microwave sounding data has always resulted in large positive impacts on the numerical weather predictions [1,2]. Since the United States launched the Television and Infrared Observation Satellite in 1978, many polar-orbiting meteorological satellites equipped with microwave sounders have been launched worldwide. In the early development stage of meteorological satellites, there were only four sounding channels for probing the atmospheric temperature profile (Microwave Sounding Unit, MSU). Since the advanced microwave sounding unit (AMSU) was firstly installed on the NOAA-15 in July 1998, the AMSU has gradually replaced the MSU, and the AMSU-A has 11 more channels than the MSU. The frequencies of channels 3, 5, 7 and 9 of the AMSU-A are similar to those of the four channels of the MSU. Moreover, the AMSU-A also includes three window channels, channels 1, 2 and 15, with the center frequencies of 23.8, 31.4 and 89 GHz, respectively. The window channel is mainly used to detect cloud and surface parameters. The additional eight channels for the middle and upper atmosphere lead to the better sounding of temperature throughout the atmosphere [3]. The polar-orbiting meteorological satellites launched by the United States and Europe are all equipped with similar microwave sounders. In China, sounders on board the polar-orbiting meteorological satellites have also advanced rapidly in recent years. From the first-generation Microwave Temperature Sounder (MWTS) on board the FY-3A/B in the early stage to the MWTS-III on board the latest polar-orbiting meteorological satellite, the FY-3E, there have been three generations of updates. The MWTS-III has more channels and provides a wider scan swath AMSU-A, and it is similar to the capability of the Advanced Technology Microwave Sounder (ATMS) [4].

In satellite data assimilation, observation errors must first be quantified, since they determine the weight of observation data relative to the background errors [5,6]. Harris and Kelly analyzed the MSU radiance data and found that a significant residual scan bias that depends strongly on latitude for some channels [7]. Lu et al. (2010) carefully evaluated the microwave sounding data on board the FY-3A satellite and found an obvious frequency drift phenomenon [8]. Through a comparison between the microwave hygrometers on board the FY-3A and the NOAA-18, Guan et al. (2011) showed that the high-altitude channels of the two microwave hygrometers have similar error characteristics [9]. Wang and Zou (2012) analyzed the error of the MWTS on board the FY-3B and found that the brightness temperatures at channel 4 had a strong anomaly in a small latitude band (30–40°N) in the northern hemisphere [10]. Then, they developed a quality control algorithm to eliminate the abnormal data. Zou et al. carefully evaluated the error characteristics of the MWTS on board the FY-3A/B and compared it with the AMSU-A. It was found that the AMSU-A biases are independent of the scene temperature, but the MWTS biases vary with the earth scene brightness temperature [11]. Han et al. (2020) evaluated the microwave sounding data from the FY-3D satellite [12] and found that there were some differences between the results of channels 4 and 11 simulated by the Community Radiative Transfer Model (CRTM) and the Radiative Transfer for TOVS (TIROS Operational Vertical Sounder) (RTTOV) models, and the long-term average deviation of the MWTS has a weak dependence on latitude. By comparing the ATMS with the AMSU-A, Weng et al. found that the ATMS temperature sounding channels have shorter integration time and therefore higher noise than the AMSU-A [4]. In this study, the data from the FY-3E MWTS-III Sounder are provided by the National Satellite Meteorological Center of China meteorological administration and are then used to analyze the error characteristics.

The remainder of this paper is organized as follows. Section 2 introduces the FY-3E/MWTS-III and the RTTOV method. In addition, it also analyzes the error characteristics of the new window channels and the error characteristics of the channels at different layers over the ocean. In Section 3, the CLWP over the ocean is retrieved based on the new channels at 23.8 and 31.4 GHz and is compared with the cloud water products from the European Centre for Medium-Range Weather Forecasts Re-Analysis 5 (ERA5). Section 4 analyzes the variation characteristics of deviation for each channel of the FY-3E/MWTS-III with the field of view (FOV) and latitude. Finally, the main conclusions are summarized in Section 5.

2. Datasets and Methods

2.1. Data Introduction

The first-generation MWTS was on board the FY-3A/B with a swath width of 2200 km and a spatial resolution of 70 km, and there were only four channels. The FY-3C was successfully launched on 23 September 2013, and the satellite-borne microwave sounder was the MWTS-II. Compared with the first generation, the improvement of the MWTS-II is mainly in the number of channels and the spatial resolution. The channels are added to 13 from 4, and the spatial resolution becomes 32 km from 70 km at the s.s.p. (sub-satellite point). On 5 July 2021, the FY-3E, the world's first early-morning-orbit satellite for civil use, was successfully launched, and the satellite-borne MWTS-III was also successfully put into use. Compared with the MWTS-II, the MWTS-III has been improved in all aspects, not only in the number of channels and spatial resolution but also in the swath width. Specially, four channels with different frequencies were added, and the swath width was increased from 2250 km to 2700 km, significantly improving the coverage of observations.

The MWTS-III inherited most of the MWTS-II features. However, four channels at the frequencies of 23.8 GHz, 31.4 GHz, 53.246 $\pm$ 0.08 GHz and 53.948 $\pm$ 0.081 GHz were added. The 23.8 GHz channel allows for more accurate estimations of the total column water vapor amount, while the 31.4 GHz channel is more sensitive to the cloud liquid water. The 53.246 ± 0.08 and 53.948 ± 0.081 GHz channels are used to supplement the temperature sounding in the troposphere at 4 km and 6 km, respectively. Compared with the MWTS-II, the sensitivity and calibration accuracy of the MWTS-III are greatly improved. Table 1 shows some channel characteristics of the MWTS-III, including channel frequency, 3-dB bandwidth, radiometric temperature sensitivity and spatial resolution. It can be found that the spatial resolution of the two newly added channels at the frequencies of 23.8 GHz and 31.4 GHz is not the same as the other channels. The nadir spatial resolution of channel 1 and 2 is 60 km, and it is 33 km for the other channels. Figure 1 shows the position of the instantaneous field of view for channel 1 and channel 7. Figure 2 exhibits the vertical distribution of the weighting function for each channel of the MWTS-III. It is indicated in Figure 2 that channels 1–4 are generally affected by surface radiation, and the rest of the channels have their weighting functions peaking in atmospheres with different heights. The highest sounding level from channel 17 is about 2 hPa.

Table 1. Parameter characteristics of each channel from the microwave temperature sounder (MWTS) on board the FY-3E.

Channel	Central Frequency (GHz)	Bandwidth (MHz)	NEΔT Minimum/Expectation (K)	Spatial Resolution (km)
1	23.8	270	0.4/0.3	60
2	31.4	180	0.45/0.35	60
3	50.3	180	0.45/0.35	33
4	51.76	400	0.3/0.3	33
5	52.8	400	0.3/0.3	33
6	53.246 ± 0.08	2 × 140	0.35/0.35	33
7	53.596 ± 0.115	2 × 170	0.3/0.3	33
8	53.948 ± 0.081	2 × 142	0.35/0.35	33
9	54.40	400	0.3/0.3	33
10	54.94	400	0.3/0.3	33
11	55.50	330	0.3/0.3	33
12	57.290344(fo)	330	0.7/0.6	33
13	fo ± 0.217	2 × 78	0.9/0.7	33
14	fo ± 0.3222 ± 0.048	4 × 36	0.9/0.8	33
15	fo ± 0.3222 ± 0.022	4 × 16	1.3/1.0	33
16	fo ± 0.3222 ± 0.010	4 × 8	1.6/1.2	33
17	fo ± 0.3222 ± 0.0045	4 × 3	2.8/2.1	33

The double (±) frequencies in column 2 mean that it is a heterodyne receiver operating in double sideband mode. The integration time of NEΔT is 16 ms.

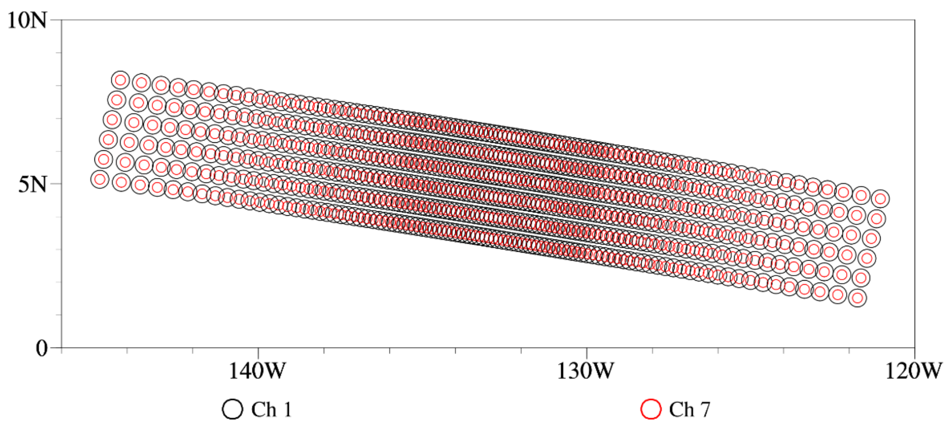

Figure 1. The position of the instantaneous field of view for channel 1 and channel 7.

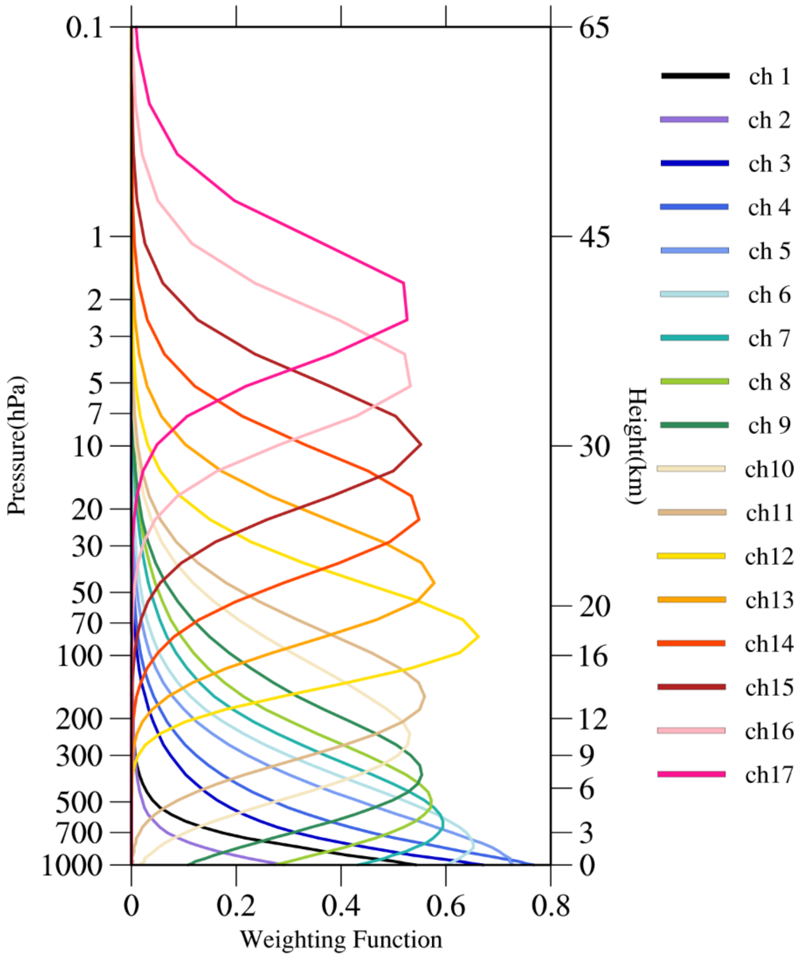

Figure 2. Weighting function of the MWTS-III. The atmospheric profile comes from the U.S. standard atmosphere. The adopted rapid radiative transfer model is the Radiative Transfer for TOVS ver.12.

Compared with the MWTS-II, the swath width and the FOV of the MWTS-III have been significantly improved. The swath width of MWTS-III increases from 2250 km to 2700 km, and the FOV number increases from 90 to 98, which significantly expands the spatial coverage of the satellite data. Figure 3 shows the spatial distributions of global brightness temperature on 17 September 2021 that were observed by channel 3 of the MWTS-III and channel 1 of the MWTS-II, which has same frequency as the former. There is an orbital gap by the MWTS-II in the latitudes between 30°N and 30°S. Meanwhile, the high and low-value areas of brightness temperature from the two instruments are almost the same, but the range of low-value areas observed by the MWTS-II is slightly larger than that observed by the MWTS-III. There are some differences in the distribution of the cold area, which is mainly concentrated on the ocean surface in the middle and high latitudes, especially on the ocean between 30–60°S. The value difference around the cold areas is about 5–10 K. The reason for this phenomenon may be the difference in observation time between the two satellites. The FY-3E is an early-morning-orbit satellite, while the FY-3D is an afternoon satellite.

The polar-orbiting satellites are flying in the solar synchronous orbit and at an altitude of about 800 km. In general, the polar-orbiting satellites can provide global observation data twice a day. Each descending or ascending orbit of the polar-orbiting satellites has a fixed local equator-crossing time. At present, the observation time of the operational polar-orbiting meteorological satellites is concentrated at about 9:30 local time (morning satellite) or 13:30 local time (afternoon satellite). In a 6-h assimilation time window, there are always 2–3 orbit coverages missing. Therefore, it is impossible to provide the global observation data only based on the morning or afternoon satellites.

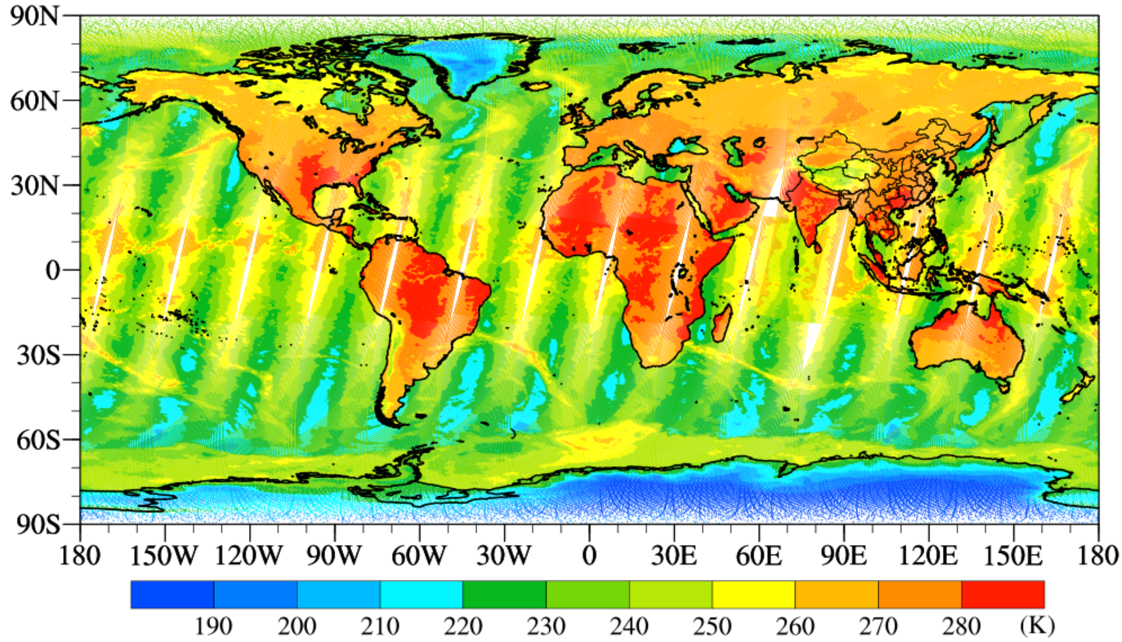

(**a**)

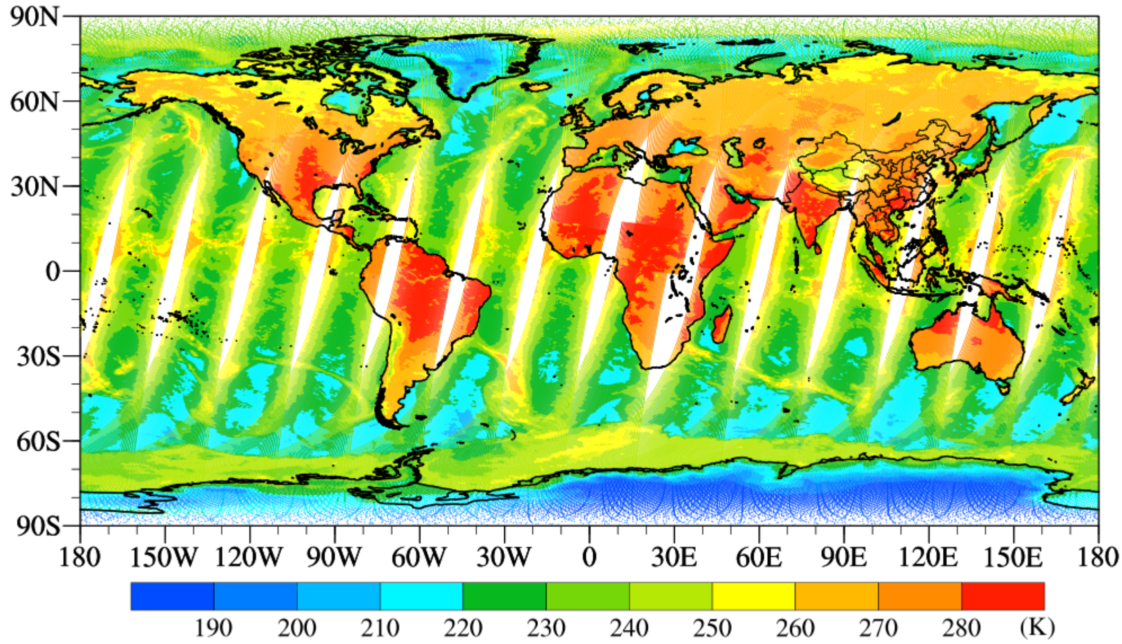

(**b**)

Figure 3. Spatial distributions of observed global brightness temperature by the channel 3 of the MWTS-III on board the FY-3E (**a**), and the channel 1 of the MWTS-II on board the FY-3D (**b**) on 17 September 2021.

The early-morning-orbit refers to the satellite observation orbit with the local time of descending node at about 0600 ETC (Equator Cross Time). The FY-3E is the first early-morning-orbit satellite for civil use independently developed by China. It not only improves and enriches the existing modern meteorological operational observation system in China but also effectively supplements the shortage of satellite observation in the 6-h assimilation window, providing a significant contribution to the prediction of the northern and southern hemispheres and the intercontinental scale regional prediction and remedying the lack of global observation data [3]. Figure 4 shows the spatial distribution of observation data by the morning satellite MetOp-A, the afternoon satellite NOAA-18 and the FY-3E in the 6-h observation assimilation time window on 17 September 2021. It can be seen that the observations of NOAA-18 and MetOp-A can effectively cover the range of China at 0000 UTC (Coordinated Universal Time) and 1200 UTC, which only have a part of the records in western China at 0600 UTC and 1800 UTC. The FY-3E can supplement the observations on the area not covered by the observations of morning and afternoon satellites and guarantee the observation of weather systems affecting China.

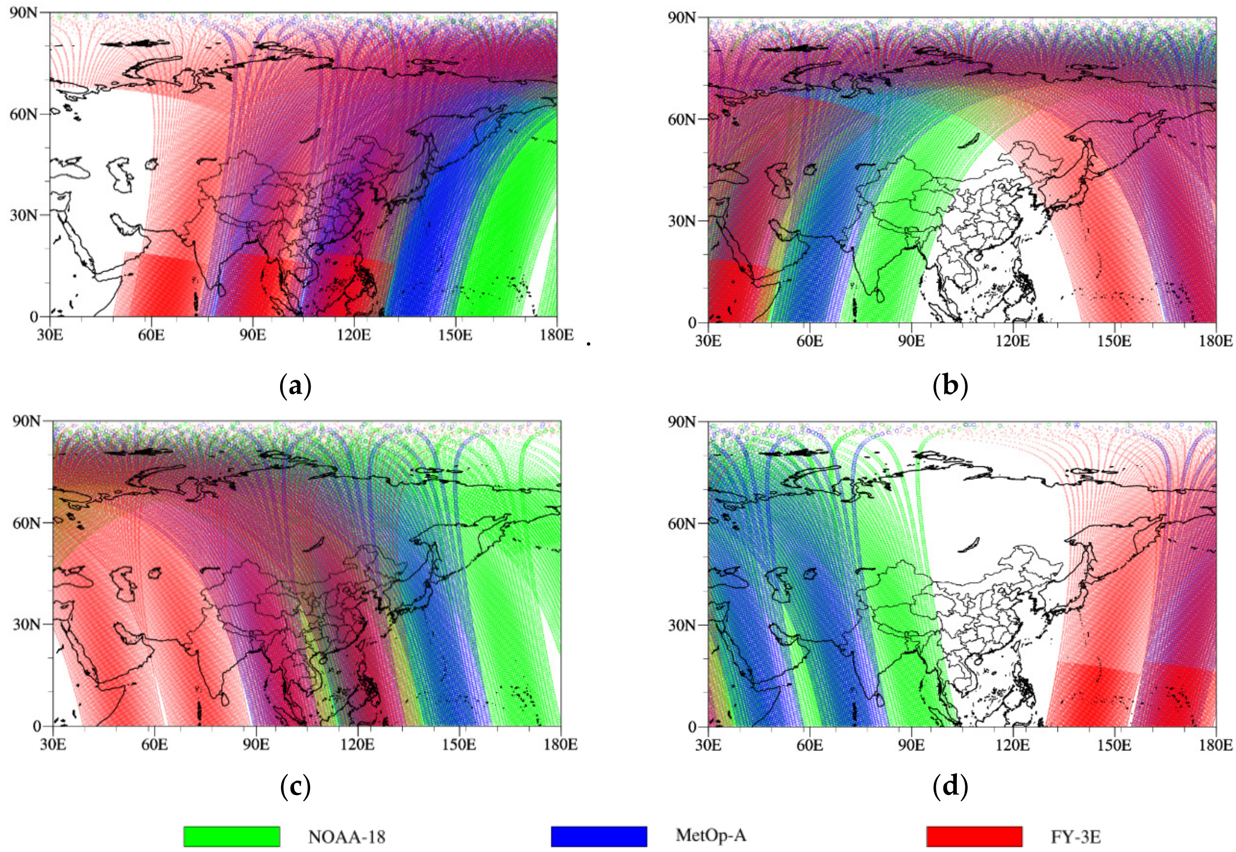

Figure 4. Observation orbits of three satellites (morning, afternoon and early-morning-orbit satellites) in the 6-h observation assimilation window at (**a**) 0000 UTC (Coordinated Universal Time), (**b**) 0600 UTC, (**c**) 1200 UTC and (**d**) 1800 UTC on 17 September 2021.

2.2. Introduction of the Radiative Transfer for TOVS Ver.12

The rapid radiative transfer model used in this study is the RTTOV model. It is developed by the European Centre for Medium-Range Weather Forecasts and has been used by many numerical weather prediction centers to assimilate the satellite data [13].

2.3. The Fifth Generation ECMWF Atmospheric Reanalysis of the Global Climate

In this study, the fifth-generation ECMWF atmospheric reanalysis of the global climate (ERA5) is used as the background field data. The ERA5 is a new generation of global reanalysis datasets from the European Centre for Medium-Range Weather Forecasts, which can provide the hourly data since 1979. The ERA5 reanalysis data include the CLWP with a horizontal resolution of about $0.25^{\circ} \times 0.25^{\circ}$. The study period in this study is from 11 to 25 September 2021.

3. Analysis of Bias and Its Standard Deviation of MWTS-III

3.1. Spatial Distributions of the Difference between Observed and Simulated Brightness Temperature at Different Heights

Before the assimilation and application, it is necessary to determine the error and deviation characteristics of the newly launched microwave instruments. In this study, the error and deviation characteristics of the MWTS-III are analyzed. To avoid the influence of the uncertainty of land surface emissivity, the study area mainly concentrates on the Pacific region in 50°S–50°N and 120°E–78°W.

Figure 5 shows the spatial distributions of differences between the observed and simulated brightness temperature (O−B) in the Pacific region for channels 1, 7 and 12 of the MWTS-III. These three channels represent the characteristics of atmospheric temperature at different heights. Channel 1 is a window channel, channel 7 is located in the middle troposphere and channel 12 is located at the tropopause. It can be seen that there are significant differences in the spatial distributions of O−B at different layers. The 23.8 GHz channel enhances the observation of the total water vapor column, which is greatly affected by weather. Therefore, the absolute value of O−B is generally large and has many small-scale characteristics. The deviation characteristics on ocean and land are significantly different, showing an alternate distribution of positive and negative values over the ocean but consistent negative deviations over the land. The peak values of the weighting functions of channel 7 and channel 12 are mainly located at 600 hPa and 100 hPa, respectively, so the spatial distributions of O−B are basically not affected by the weather. However, the spatial distribution characteristics of O-B are not the same. Channel 7 shows a consistent negative deviation in the Pacific, and the values in most regions are between −3 K and −1 K. It can also be observed that there are some large negative value areas in the central Pacific region of 10°N, which show a large positive value in channel 2 but do not exist in channel 12. This shows that there are relatively deep clouds in this area, which have affected the height of 600 hPa. In the Pacific, the absolute value of the O-B of channel 12 is less than that of 2 K, and most areas show positive deviation, while the negative values mainly concentrate over the tropical areas. Comparing the O-B characteristics of three channels with different heights, it can be found that the error characteristics of the three channels are different, and the factors affecting the error of each channel are also different. These factors also need to be taken into account when analyzing the bias characteristics of different channels.

3.2. Retrieval of CLWP by the FY-3E/MWTS Observation

Although the homogeneous surface type in the ocean can greatly reduce the surface emissivity errors from affecting the error estimation results, it is still vulnerable to the influence of clouds. The effective identification of cloudy-sky satellite data is also an essential prerequisite for error analysis and data assimilation [14]. Whether it is clear-sky assimilation or full-sky assimilation, the effective discrimination of clear-sky data and cloudy-sky data can provide the appropriate observation error characteristics [15,16]. In the MWTS-III, the 23.8 GHz and 31.4 GHz channels are added. Previous studies have developed the CLWP retrieval method based on the observed brightness temperature of these two channels, which provides an effective means for the cloud detection of the MWTS-III data. According to the microwave observation of the window channel with a low frequency, the cloud liquid water in the non-precipitation cloud can be calculated [17–21]. Weng et al. (2003) proposed that the CLWP and total precipitable water can be calculated based on the observed brightness temperature, sea surface temperature and wind field at the 23.8 and 31.4 GHz window channels of the AMSU-A [22]. Therefore, in this study, the newly added 23.8 and 31.4 GHz channels on the FY-3E/MWTS are used to carry out the retrieval experiments of the CLWP over the ocean. Based on the method proposed by Weng et al. (2003) [22], the reanalysis data of the sea surface temperature and wind field are interpolated into the observation points of the satellite through the Lagrange interpolation, and then the CLWP is retrieved.

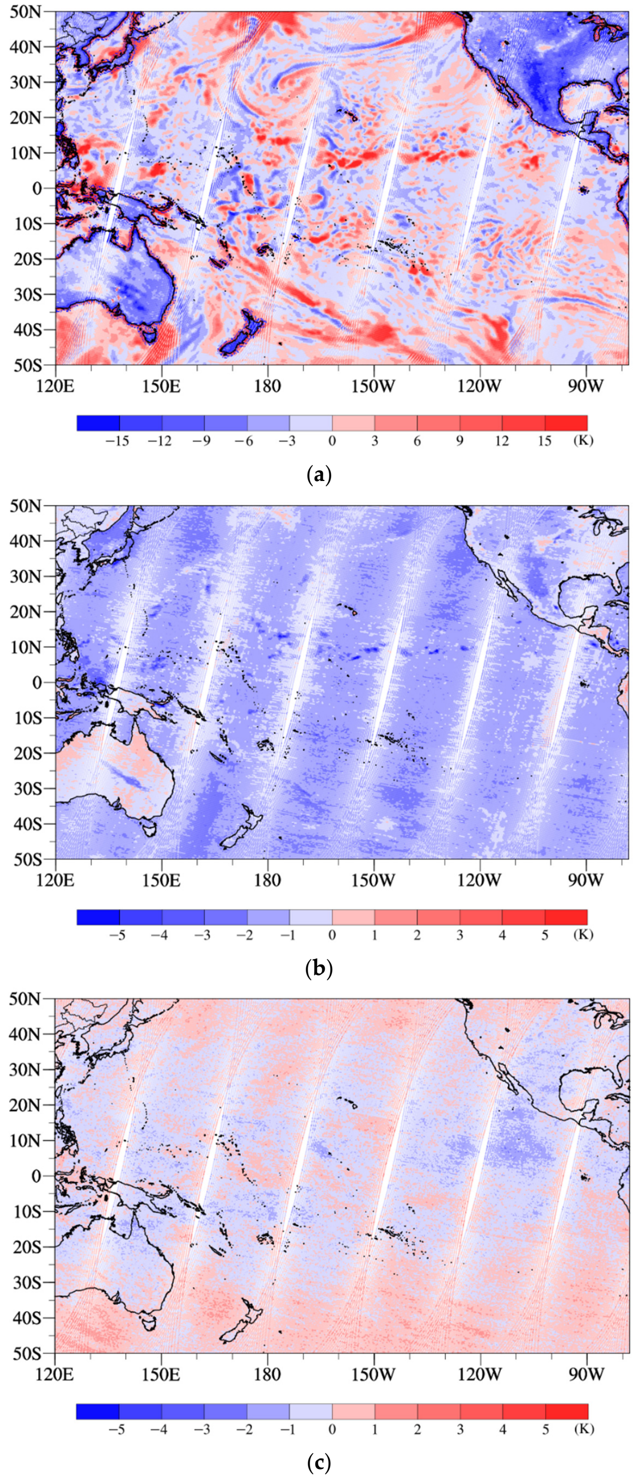

Figure 5. Spatial distributions of the difference between the observed and simulated brightness temperature (O−B) in the Pacific region for (**a**) channel 1, (**b**) channel 7 and (**c**) channel 12 of the MWTS-III on 17 September 2021.

Figure 6a shows the spatial distribution of the retrieved CLWP from the MWTS-III observation in the Pacific region on 17 September 2021. The gray area represents the CLWP below 0.02 kg·m^{-2}, and the white area is with missing observations. To verify the accuracy of the retrieval products, the cloud liquid water product from the ERA5 at the same time is shown in Figure 6b. For the convenient comparison between them, the cloud liquid water product of the ERA5 at the corresponding time has been interpolated to the satellite observation points. It takes the satellite a certain time to cover the whole Pacific Ocean, and the cloud liquid water path will also change significantly during this time. Therefore, in order to ensure a better time correspondence between the ERA5 and the observation data, for each observation data, we have to select the ERA5 reanalysis data closest to the observation time from the hourly ERA5 data and interpolate it to the observation position. At the same time, in order to ensure the consistent resolution of the two data, the interpolation method chosen is the spatial average method. The CLWPs of the ERA5 within 60×60 km around each observation are spatially averaged as the CLWPs of the ERA5 corresponding to that observation. Through the comparison, it can be found that the distributions of cloud liquid water are similar. Especially, the high-value areas of the two are close, which mainly locate in 10°N, 40–50°N and 40–50°S. The larger the CLWP is, the thicker the clouds are, which may be due to the more deep convective clouds. However, in terms of the magnitude, the value of the retrieval product is slightly larger than that of the reanalysis data. It can be found that the value of 0.02–0.04 kg·m^{-2} exists in a wide region for the ERA5 cloud liquid water product, where the CLWP value of the MWTS-III retrieval product is less than 0.02 kg·m^{-2}.

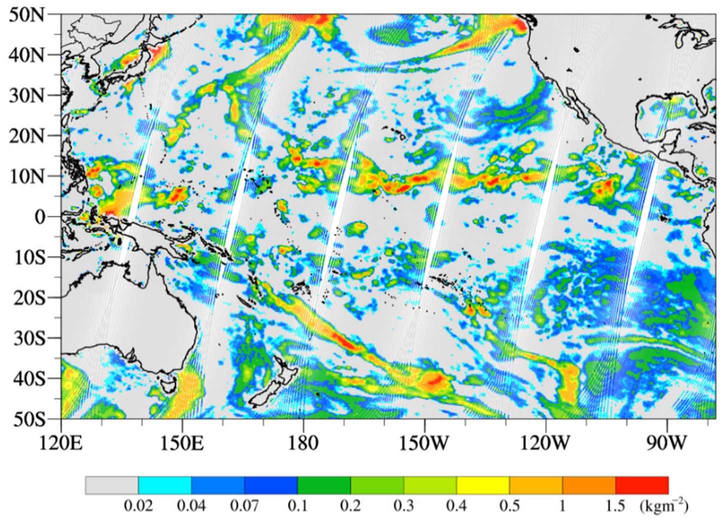

(**a**)

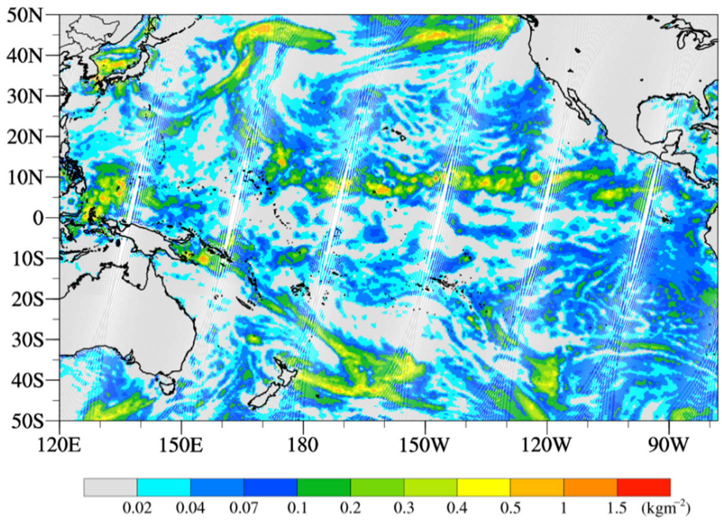

(**b**)

Figure 6. Spatial distributions of cloud liquid water path (CLWP) from (**a**) the retrieval of the MWTS-III and (**b**) the ERA5 over the Pacific region on 17 September 2021.

To more obviously compare the difference between the clear-sky points obtained by the MWTS-III retrieval products and the CLWP products from the ERA5, the cloud detection of the microwave sounding data is carried out based on these two CLWPs. According to the standards of previous research, the clear-sky data are defined as the data with the CLWP below 0.02; otherwise, it is considered as cloudy-sky data [23]. Then, the O−B standard deviations from each channel in the clear-sky areas are calculated, and the results are shown in Figure 7.

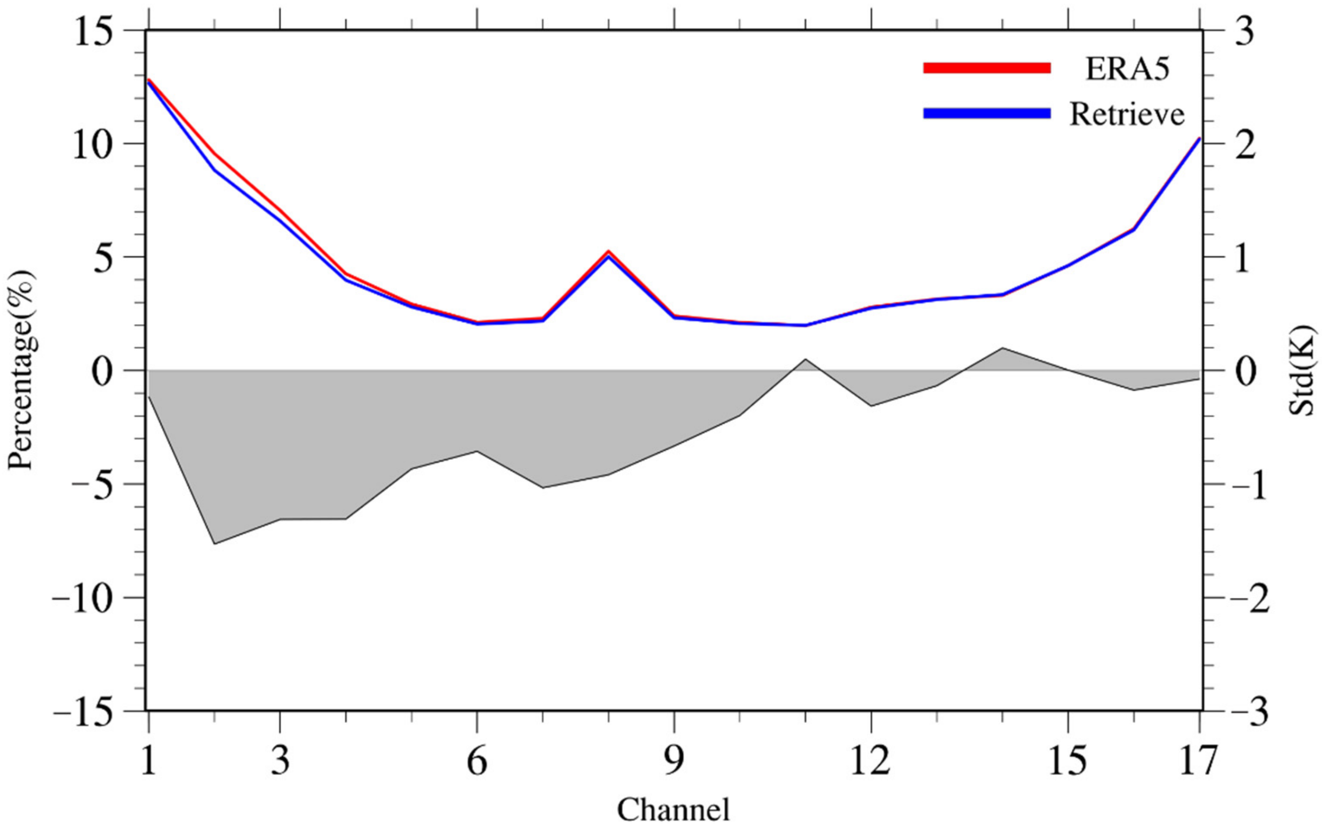

Figure 7. Standard deviations of O−B at clear-sky points from each channel over the Pacific region from 11 to 25 September 2021. The standard deviation for the MWTS-III and the ERA5 (red line and blue line, right scale); Difference between the deviations for the MWTS-III and the ERA5 (black line and shaded region, left scale).

Figure 7 displays the standard deviations of O−B at the clear-sky points for each channel based on the cloud detection of the CLWP products from the MWTS-III retrieval and the ERA5. To further eliminate the impact of abnormal data on the statistical results, the abnormal data with an absolute value of O−B above 5.0 K are excluded. It can be seen from the results that, for the high-level channels (channels 11–17), the results obtained by the two methods are similar, with the difference within 1%. This is because the high-level channel is not sensitive to clouds. However, for the low-level channels (channels 1–10), the standard deviation obtained by the cloud detection method based on the MWTS-III retrieved CLWP is noticeably less than that obtained by the cloud detection of the ERA5 CLWP product. Especially, the disparity for channels 2–4 is more significant. The difference between the standard deviations reaches about 7%, which is about 4% for other low-level channels. It can be seen that the improvement of the O−B from low-level channels of the FY-3E based on the retrieved CLWP is effective, which also reveals that the performance of cloud detection based on the retrieval of observation data is better than that based on the reanalysis data if used for the cloud detection of the MWTS-III observation data. Of course, we also need to acknowledge that, here, the ERA5 CLWP is interpolated to the observation points, and there must be a resolution difference, which may be one of the reasons why the retrieval product works slightly better. More importantly, the CLWP of the reanalysis data is not available in real-time assimilation. The results here can prove that the co-located cloud detection based on the retrieval of observation data can meet the needs of real-time assimilation well.

4. O-B Variation Characteristics with MWTS-III Field of View and Regions

One of the characteristics of the cross-track scanning instrument is that the observed value changes with the scanning angle. This is due to the variation of the optical path and the weighting function peak with a scanning angle. After eliminating abnormal data by the cloud detection and quality control methods, the variations of the average and standard deviations of O-B from each channel ascending and descending orbit with the FOV from 11 to 25 September 2021 are presented in Figure 8.

The left column of Figure 8 shows that the average of O-B at different channels mainly concentrates between ± 2 K. Only the deviations of channels 8 and 10 are negative, with the value between -2 K to -3 K. The difference in the average of O-B at ascending and descending orbit is small. They have a similar trend, but there are some differences in value, which is basically less than 0.1 K.

The right column of Figure 8 shows the variation curve of the standard deviation of O-B with the FOV. The standard deviation of O-B for each channel is less than 1.5 K. The standard deviations are between 1–1.5 K in channels 1–3 and 17, and the maximum of 1.5 K is reached in channel 1. Through the comparison of the standard deviations in the channels at different layers, it is found that the standard deviation of the channels 5–11 is the smallest, with the value being basically between 0.3–0.6 K. Similar to the characteristics of the average of O-B at ascending and descending orbit, the difference in the standard deviation of O-B at ascending and descending orbit is still small. In addition, we also found that the average and the standard deviation of O-B from the channels 1–10 shows a prominent symmetrical variation characteristic with the FOV from Figure 7. Additionally, there is an obvious fluctuation with the FOV, especially for the average of channels 14–17 and the standard deviation of channels 16 and 17.

There are differences in the FOV of satellites at different latitudes due to the spherical characteristics of the earth, causing different error and deviation characteristics of the satellite observation data at different latitudes. Figure 9 shows the variations of the average and standard deviations of O-B with latitude. It can be seen that the variation range of the average O−B in different channels at different latitudes is basically between -2 K to 2 K. The averages of O-B in channels 4, 7, 8 and 10 are negative, while they are positive in channels 15–17. The standard deviations of O-B in most channels are less 1.0 K, but they are 1–1.5 K in channels 1–4 and 17. Similar to the results in Figure 8, there is still no significant difference between ascending and descending orbit. The average and standard deviation of O-B in most channels does not change significantly with latitude. The absolute values of average O-B to the north of 20°N in some channels decrease slightly, and the standard deviation increases with latitude in channels 3–7. Especially, the standard deviation increases by 0.3 K for channel 4 and 0.1 K for channel 5. However, in the south of 20°N, the average and standard deviations do not vary significantly with latitude. For channels 11–17, where the peak of weighting function is located at the tropopause and stratosphere, the variation magnitude of the average and standard deviations of O−B with latitude is relatively small.

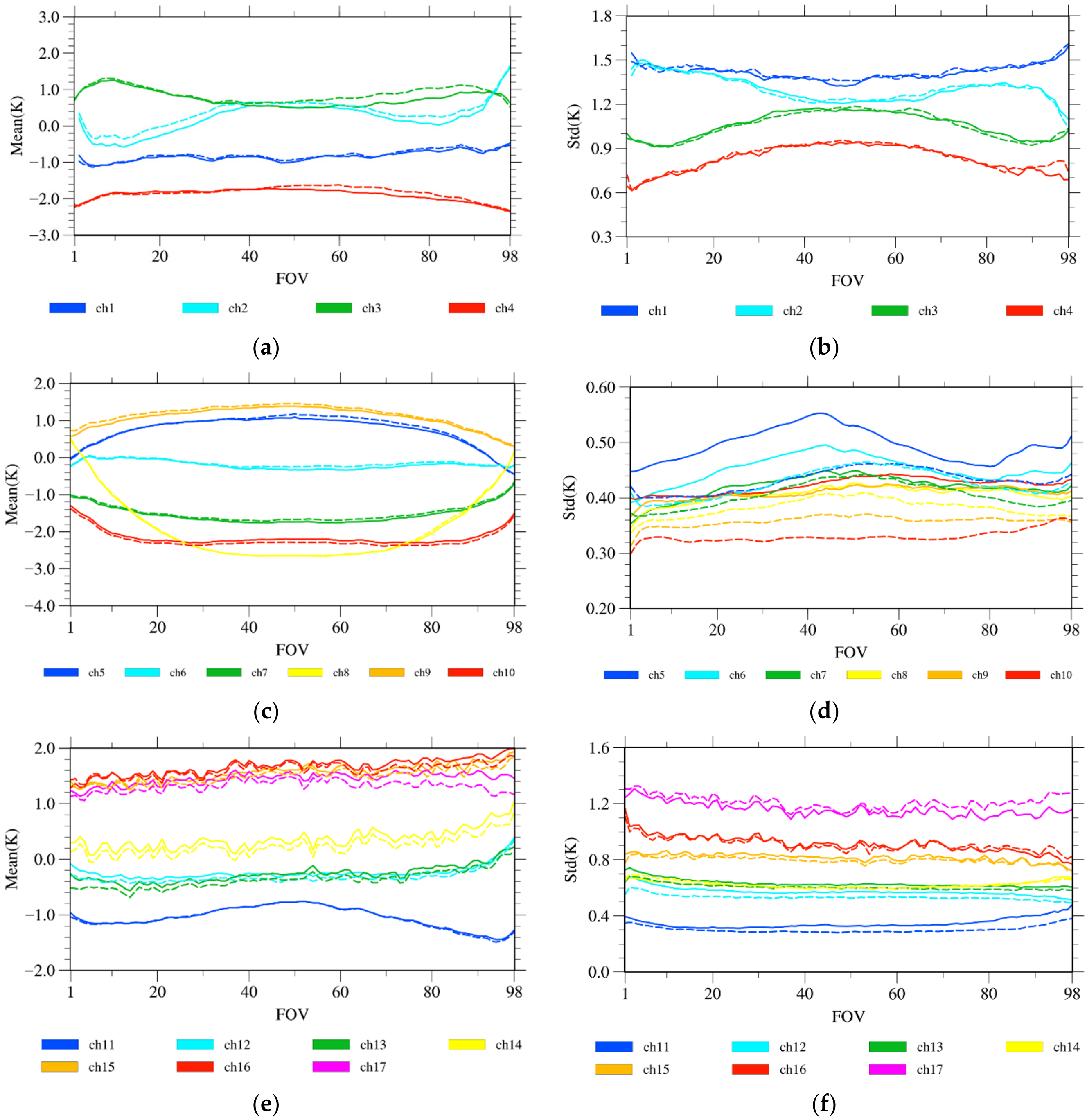

Figure 8. Variations of the (**a**,**c**,**e**) average and (**b**,**d**,**f**) standard deviation of O−B with the field of view (FOV) for each channel over the Pacific region from 11 to 25 September 2021. (solid line: ascending orbit; dashed line: descending orbit).

However, it should be pointed out that the results here are only obtained based on the data of two weeks, and the influence of weather systems is unavoidable, especially the obvious change of bias and s.t.d. In the north of 20°N, this may also be the reason for the insufficient effect of cloud detection due to the complexity of the mid latitude weather system. For channels 11–17, where the peak of the weighting function is located at the tropopause and stratosphere, these channels are basically not affected by the cloud, and this feature basically does not exist.

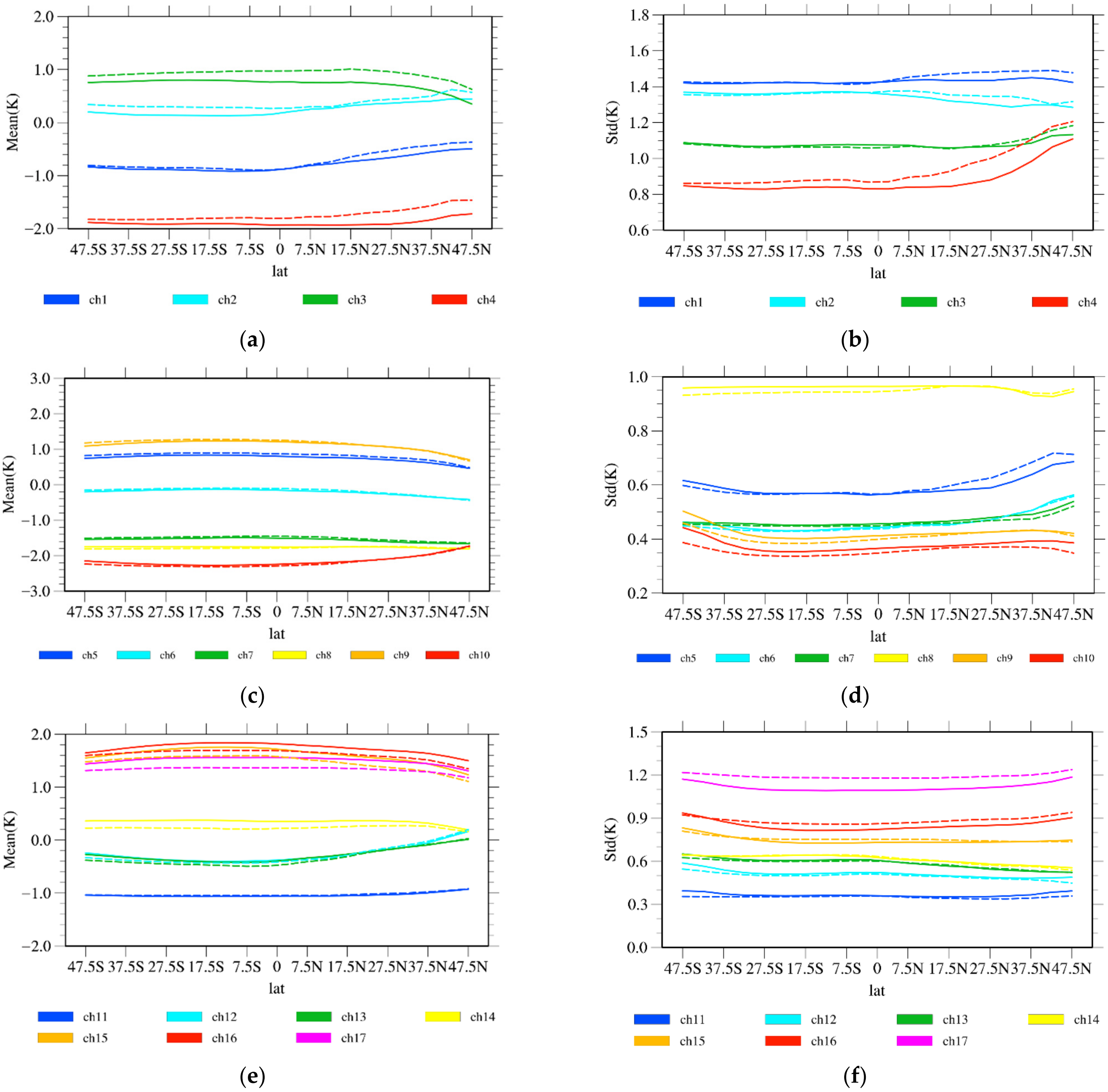

Figure 9. Variations of (**a**,**c**,**e**) the average and (**b**,**d**,**f**) standard deviations of O−B for each channel of the MWTS-III over the Pacific region with latitude from 11 to 25 September 2021. (solid line: ascending orbit; dashed line: descending orbit).

5. Discussion and Conclusions

The FY-3E is the world's first early-morning-orbit satellite independently developed by China. It improves and enriches the existing modern meteorological operational observation system in China and effectively supplements the shortage of satellite observation in a 6-h assimilation window. Determining the error characteristics is essential for the assimilation application of the MWTS data from the FY-3E.

In this study, the error and deviation characteristics over the Pacific region are analyzed. Based on the new channels of 23.8 and 31.4 GHz, the CLWP over the ocean areas is successfully retrieved. The cloudy-sky data is recognized based on the retrieved CLWP. Finally, the variation characteristics of O−B from different channels in clear-sky with the FOV and latitude are analyzed in detail.

The results show that the retrieved CLWP based on the newly added 23.8 and 31.4 GHz channels can effectively recognize the cloudy-sky and clear-sky data over the ocean. For the clear-sky data, the average of O−B from different channels mainly concentrates between ±2 K. There are large negative deviations for channels 8 and 10. The standard deviations of O−B in different channels are all below 1.5 K, and they are between 0.3–0.6 K for the channels 5–11, which is significantly lower than those of the channels at other heights. The average and the standard deviation of O−B from the channels 1–10 shows an obvious symmetrical variation with the FOV. There is an apparent fluctuation with the FOV for the average of channels 14–17 and the standard deviation of channels 16 and 17.

The average and standard deviations of O−B vary with the latitude in the north of 20°N for the channels 3–7. The average of O−B decreases with the latitude, but the standard deviation increases with the latitude, especially for channels 4 and 5. The standard deviations of O−B in the channels 11–17 are stable, with an apparent variation characteristic with latitude.

In general, the early-morning orbit makes the microwave sounder of the FY-3E complement the present morning and afternoon satellite very well, and the two additional window channels provide good conditions for the identification of clear sky and cloudy data for the satellite data assimilation. The stable bias and error characteristics provide a good basis for the effective assimilation of this data, so the evaluation results all indicate that the assimilation of the microwave sounding data of the FY-3E can make valuable contributions to the improvement of numerical weather prediction.

In this study, only the observation data of the MWTS-III on board the FY-3E for half a month are used to analyze the error characteristics over the ocean. In future studies, the long-term observation data of the MWTS-III will be used to analyze the error characteristics on the land.

Author Contributions: Conceptualization, J.L.; methodology, Z.Q.; software, X.Q.; validation, J.L., Z.Q. and G.L.; formal analysis, X.Q.; investigation, X.Q.; data curation, G.L.; writing—original draft preparation, X.Q.; writing—review and editing, Y.H. and J.L. All authors have read and agreed to the published version of the manuscript.

Funding: This research was jointly funded by the National Key R&D Program of China (Grant 2018YFC1507302), the Youth Project of the National Natural Science Foundation of China (41805076), the Natural Science Foundation of Jiangsu Province (BK20211396) and the Fengyun Application Pioneering Project (FY-APP-2021.0201).

Data Availability Statement: All data used in this paper are available from the authors upon request (20191201014@nuist.edu.cn).

Acknowledgments: The authors would like to acknowledge the National Satellite Meteorological Centre of CMA for providing the satellite data.

Conflicts of Interest: The authors declare no conflict of interest.

References

1. Eyre, J.R. Progress Achieved on Assimilation of Satellite Data in Numerical Weather Prediction over the Last 30 Years. In Proceedings of the ECMWF Seminar on Recent Developments in the Use of Satellite Observations in Numerical Weather Prediction, Reading, UK, 3–7 September 2007; ECMWF Publication: Reading, UK, 2007; pp. 1–27.
2. Bao, Y.; Xu, J.; Powell, A.M., Jr.; Shao, M.; Min, J.; Pan, Y. Impacts of AMSU-A, MHS and IASI data assimilation on temperature and humidity forecasts with GSI–WRF over the western United States. *Atmos. Meas. Technol.* **2015**, *8*, 4231–4242. [CrossRef]
3. Zhang, P.; Hu, X.; Lu, Q.; Zhu, A.; Lin, M.; Sun, L.; Chen, L.; Xu, N. FY-3E: The first operational meteorological satellite mission in an early morning orbit. *Adv. Atmos. Sci.* **2022**, *39*, 1–8. [CrossRef]
4. Weng, F.; Zou, X.; Wang, X.; Yang, S.; Goldberg, M.D. Introduction to Suomi national polar-orbiting partnership advanced technology microwave sounder for numerical weather prediction and tropical cyclone applications. *J. Geophys. Res.* **2012**, *117*, D19112. [CrossRef]
5. Waller, J.A.; Dance, S.L.; Nichols, N.K. Theoretical insight into diagnosing observation error correlations using observation-minus-background and observation-minus-analysis statistics. *Q. J. R. Meteorol. Soc.* **2016**, *142*, 418–431. [CrossRef]
6. Chapnik, B.; Desroziers, G.; Rabier, F.; Talagrand, O. Diagnosis and tuning of observational error in a quasi-operational data assimilation setting. *Q. J. R. Meteorol. Soc.* **2006**, *132*, 543–565. [CrossRef]

7. Harris, B.A.; Kelly, G. A satellite radiance-bias correction scheme for data assimilation. *Q. J. R. Meteorol. Soc.* **2001**, *127*, 1453–1468. [CrossRef]
8. Lu, Q.; Bell, W.; Bauer, P.; Bormann, N.; Peubey, C. An initial evaluation of FY-3A satellite data. *ECMWF Technol. Memo.* **2010**, *631*, 58.
9. Guan, L.; Zou, X.; Weng, F.; Li, G. Assessments of FY-3A microwave humidity sounder measurements using NOAA-18 microwave humidity sounder. *J. Geophys. Res.* **2011**, *116*, D10106. [CrossRef]
10. Wang, X.; Zou, X. Quality assessments of Chinese Fengyun-3B microwave temperature sounder (MWTS) measurements. *IEEE Trans. Geosci. Remote Sens.* **2012**, *50*, 4875–4884. [CrossRef]
11. Zou, X.; Wang, X.; Weng, F.; Li, G. Assessments of Chinese Fengyun microwave temperature sounder (MWTS) measurements for weather and climate applications. *J. Atmos. Ocean. Technol.* **2011**, *28*, 1206–1227. [CrossRef]
12. Han, Y.; Hou, X. Evaluation of the in-orbit performance of the microwave temperature sounder onboard the FY-3D satellite using different radiative transfer models. *J. Quant. Spectrosc. Radiat. Transf.* **2020**, *253*, 107041. [CrossRef]
13. Saunders, R.; Hocking, J.; Turner, E.; Rayer, P.; Rundle, D.; Brunel, P.; Vidot, J.; Roquet, P.; Matricardi, M.; Geer, A.; et al. An update on the RTTOV fast radiative transfer model (currently at version 12). *Geosci. Model Dev.* **2018**, *11*, 2717–2737. [CrossRef]
14. Bormann, N. *Modification of AMSU—A Quality Control to Reintroduce Tropospheric Channels from NOAA-16 and Aqua*; ECMWF Research Department Internal Memorandum: Reading, UK, 2008.
15. Bauer, P.; Geer, A.J.; Lopez, P.; Salmond, D. Direct 4D-Var assimilation of all-sky radiances: Part I. Implementation. *Q. J. R. Meteorol. Soc.* **2010**, *136*, 1868–1885. [CrossRef]
16. Geer, J.A.; Bauer, P. Observation errors in all-sky data assimilation. *Q. J. R. Meteorol. Soc.* **2011**, *137*, 2024–2037. [CrossRef]
17. Greenwald, T.J.; Stephens, G.L.; Vonder Haar, T.H.; Jackson, D.L. A physical retrieval of cloud liquid water over the global oceans using Special Sensor Microwave/Imager (SSM/I.) observations. *J. Geophys. Res.* **1993**, *98*, 18471–18488. [CrossRef]
18. Weng, F.Z.; Grody, N.C. Retrieval of cloud liquid water using the Special Sensor Microwave Imager (SSM/I). *J. Geophys. Res.* **1994**, *99*, 25535–25551. [CrossRef]
19. Weng, F.; Grody, N.C.; Ferraro, R.; Basist, A.; Forsyth, D. Cloud liquid water climatology derived from the special sensor microwave imager. *J. Clim.* **1997**, *10*, 1086–1098. [CrossRef]
20. Weng, F.; Ferraro, R.R.; Grody, N.C. Effects of AMSU Cross-Scan Asymmetry of Brightness Temperatures on Retrieval of Atmospheric and Surface Parameters. In *Microwave Radiometry and Remote Sensing of the Earth's Surface and Atmosphere*; Pampaloni, P., Paloscia, S., Eds.; CRC Press: Boca Raton, FL, USA, 2000; pp. 255–262.
21. Wentz, F.J. A well-calibrated ocean algorithm for special sensor microwave/imager. *J. Geophys. Res.* **1997**, *102*, 8703–8718. [CrossRef]
22. Weng, F.; Zhao, L.; Ferraro, R.; Poe, G.; Li, X.; Grody, N.C. Advanced microwave sounding unit cloud and precipitation algorithms. *Radio Sci.* **2003**, *38*, 8068. [CrossRef]
23. Lin, B.; Minnis, P.; Fan, A. Cloud liquid water path variations with temperature observed during the surface heat budget of the arctic ocean (SHEBA) experiment. *J. Geophys. Res.* **2003**, *108*, 4427. [CrossRef]